



## Catalytic Conversion of Beef Tallow to Biofuels using MgO Nanoparticles Green Synthesized by Zingiber officinale Roscoe Rhizome Extract

Adi Riyadh<sup>1,2\*</sup>, Yoki Yulizar<sup>1</sup>, Bambang Heru Susanto<sup>3</sup>

<sup>1</sup>Department of Chemistry, Faculty of Mathematics and Natural Sciences, Universitas Indonesia, Depok 16424, Indonesia

<sup>2</sup>Department of Chemistry, Faculty of Science and Technology, Universitas Islam Negeri Syarif Hidayatullah, Tangerang selatan 15412, Indonesia

<sup>3</sup>Department of Chemical Engineering, Faculty of Engineering, Universitas Indonesia, Depok 16424, Indonesia

**Abstract.** MgO nanoparticles (MgONPs) have been successfully synthesized using ZOE (Zingiber officinale Roscoe extract in water) and applied for catalytic conversion of beef tallow to biogasoline, kerosene, and diesel. ZOE was used due to containing the alkaloid as a weak base source to hydrolyze  $Mg(NO_3)_2$  precursor and form the MgONPs. The synthesized MgONPs were characterized using UV-Vis spectrophotometer, X-ray diffraction (XRD), particle size analyzer (PSA), Brunauer–Emmett–Teller (BET) surface areas. UV-Vis diffuse reflectance spectrophotometry (DRS), scanning electron microscopy-energy dispersive X-ray spectroscopy (SEM-EDX), and transmission electron microscopy (TEM). The catalyst activity was performed to convert beef tallow to biofuel in the stainless-steel reactors at 300 °C for 60 min. The conversion results of beef tallow were analyzed using gas chromatography-mass spectrometry (GC-MS). The beef tallow conversion shows that all fatty acids derived from beef tallow are converted to gases and liquids fractions. The conversion using a catalyst to feed weight ratio of 4 wt. % produced the liquid fractions containing the dominant alkanes (62.85%) and cyclic compounds (18.77%). Pentadecane and Heptadecane are liquid products' main compounds, indicating a decarboxylation reaction.

**Keywords:** Beef tallow; Decarboxylation; MgO Nanoparticles; Zingiber officinale Roscoe

### 1. Introduction

Fatty acids derived from animals and plants can be converted into hydrocarbons through the process of cracking (Nasikin et al., 2009), deoxygenation (Susanto et al., 2016; Muharam & Soedarsono, 2020), decarboxylation (Wu et al., 2016). Using catalysts, and decarbonylation (Dawes et al., 2015) to gasoline, kerosene, and diesel. The MgO catalyst prepared from magnesium oxalate was studied by Khromova et al. (2013) and is useful for decarboxylation of pentanoic acid to dibutyl ketone. MgO catalysts are also useful for the decarboxylation reaction of naphthenic acid from crude oil in petroleum (Zhang et al., 2006). MgO catalysts encourage the decarboxylation of fatty acids into hydrocarbons and  $CO_2$  (Natewong et al., 2016; Dickerson & Soria, 2013). Decarboxylation of oleic acid occurs at 300 °C decarboxylation and pyrolysis reactions occur at 350 °C while the dominant pyrolysis reaction is it 400 °C (Roh et al., 2011). Leong et al. (2016) also reported that the

\*Corresponding author's email: [adikimia@uinjkt.ac.id](mailto:adikimia@uinjkt.ac.id), Tel.: (62-21)7493606, Fax.: (62-21)7493315  
doi: [10.14716/ijtech.v13i4.4821](https://doi.org/10.14716/ijtech.v13i4.4821)

highest yield of the liquid fraction from the crude glycerol pyrolysis result was obtained at a temperature of 400°C. The mechanism of magnesium oxides as a catalyst in the decarboxylation of acids has been studied in works (Perera et al., 2015; Na et al., 2010; Gasanov et al., 2013; Diez et al., 2000). Strong chemisorption of a carboxyl group (–COOH) on the MgO surface leads to a decarboxylation reaction (Perera et al., 2015). Nanocatalysts can be used to increase the yield and performance of biofuel production. Various nanotechnology applications depend on nano-size properties, morphology, and surfaces reactivity (Sekoai et al., 2019). MgO nanoparticle catalysts can be synthesized using plant extracts, and this method continues to be developed due to using environmentally friendly materials. Some plant extracts that have been studied for MgO NPs synthesis include the Neem leaf plant (Moorthy et al., 2015), Rosemary flower (Abdallah et al., 2019), Cajanus cajan leaf (Surya et al., 2021), and Trigonella foenum-graecum leaves extracts (Vergheese & Vishal, 2018).

Rhizome Ginger (*Zingiber officinale Roscoe*) is an Indonesian spice that is very important in everyday life, especially in health. Ginger is a medicinal plant that contains alkaloids (Riaz et al., 2015). Alkaloids are a group of the weak organic base that is mostly heterocyclic and found in plants. Alkaloids can form salts when reacting with acids. Alkaloids content in dried ginger (*Zingiber officinale Roscoe*) is 5.86% (w/w) (Raaof et al., 2013). Ginger extract has been widely used as auxiliary material for nanomaterial synthesis. Ginger extract was used to synthesize AgNPs with particle sizes of 10-20 nm (Velmurugan et al., 2014) and AuNPs with the size of 5-20 nm (Yang et al., 2017). Ginger extract has a high alkaloid content and potency for nanoparticle formation of MgO. In forming metal oxide, nanoparticles need a weak base source as an alkaloid in the plant extract for hydrolyzing metal ion to metal hydroxide, finally forming metal oxide nanoparticles after calcination (Yulizar et al., 2018). This study aimed to develop an effective and efficient catalyst at low temperatures to produce biogasoline, kerosene, and diesel from beef tallow. MgONPs synthesis used white ginger extract (*Zingiber officinale Roscoe*) as a weak base and  $Mg(NO_3)_2$  as a precursor. Catalyst characterization and chemical properties of products are carried out using some chemical instrumentations. MgONPs catalyst activity was conducted on the conversion of beef tallow to biogasoline, kerosene, and diesel productions.

## 2. Materials and Methods

### 2.1. Materials

White ginger rhizome (*Zingiber Officinale Roscoe*) was obtained from Nagrak Sukabumi West Jawa, Indonesia. Identification of ginger rhizomes was carried out at the biology research center, Bogor, West Java, Indonesia. Beef tallow was obtained from the household industry in Kemang Bogor, West Java, Indonesia. Beef tallow is a product of beef fat hydrolysis that has been separated from muscle tissue, meat, and bone residues.  $Mg(NO_3)_2$  was purchased from Merck as a precursor of MgONPs synthesis. Commercial MgO was obtained from Merck for comparison of catalytic performance.

### 2.2. Extraction of White Ginger Rhizomes

Rhizome ginger was washed and sliced thinly, then dried by winding under the visible light for two weeks. The dried ginger was mashed into powder. Ginger extraction was done using Soxhlet with methanol. Soxhlet extraction temperature was done at the standard boiling point of methanol at 64.7°C for 8 hours. The extracts are filtered using Whatman no. 1 and partitioned with n-hexane. The methanol fraction was concentrated using a rotary evaporator and dissolved in water.

The white ginger powder was extracted using methanol to dissolve polar and semi-polar chemical compounds. The crude methanol extract was partitioned using n-hexane

(1:1) to remove non-polar compounds, then the methanol fraction separated. A concentrated extract of methanol was added to demineralized water to obtain a water fraction of white ginger extract with a concentration of 1%. Phytochemical screenings were conducted to determine the content of secondary metabolites in ZOE (Zingiber officinale Roscoe extract in water), and the result showed the presence of alkaloids, terpenoids, flavonoids, and saponins.

### 2.3. Synthesis MgONPs using Zingiber Officinale Roscoe extract

Synthesis of MgONPs was done by adding 1500 mL of  $Mg(NO_3)_2$  10 mM and 75 mL of ZOE 1% (w/v), then stirred and heated at 80°C for four h. During the Synthesis MgONPs reaction at 60,120,180 and 240 min, the formed colloids were observed using UV-Vis spectrophotometer. The formed colloids were dried in an oven at 120 °C for 48 h and calcined at 800°C for two h to form MgONPs.

According to [Suresh et al. \(2018\)](#), magnesium nitrate precursors react with secondary metabolite compounds in plant extracts to form complex compounds with weak hydrogen bonding. When a complex colloid of Mg-phytochemicals is heated in the oven, there is a conversion into magnesium hydroxide. Calcinating magnesium hydroxide complex formed magnesium oxide nanoparticles ([Suresh et al., 2018](#)). This study predicted secondary metabolite compounds that play a role in the formation of nanoparticles are alkaloid group compounds. The presence of alkaloids plays a role in MgONPs synthesis that acts as a weak base source, while flavonoids and terpenoids as capping agents, and saponins as biosurfactants for bio templates ([Noruzi, 2015](#); [Pugazhendhi et al., 2019](#); [Judith Vijaya et al., 2017](#)).

### 2.4. Catalyst characterization

X-ray diffraction (XRD) analysis was performed to identify the structure crystallography of metal oxide catalysts using Diffractometer Shimadzu XRD-7000. The specific surface area and distribution of catalyst pores were determined by the Brunauer-Emmet-teller (BET) method with the  $N_2$  adsorption/desorption analyzer using ASAP 2020 Micromeritics Instrument Corp. The morphology and composition of Mg and O elements in MgO NPs catalysts were determined by SEM-EDX using JED-2300. UV-VIS absorption spectrum of colloid was conducted using a Spectrophotometer UV-VIS (Shimadzu 2600) in the range of 200-800 nm. The bandgap values were investigated using UV-Vis diffuse reflectance spectroscopy (DRS, Agilent Technologies Cary 60). A transmission electron microscopy (TEM) image was taken by TEM (JEOL JEM 1400). GC-MS was performed using Perkin Elmer GC Clarus 680 and MS Clarus SQ 8 T. Particle size distribution was done by particle size analyzer (PSA) zeta sizer nano series (Malvern Zetasizer ZEN-1600).

### 2.5. Conversion of beef Tallow to Biofuel

The conversion of beef tallow was done using the catalyst of MgONPs compared with commercial MgO. The reaction was carried out using a stainless-steel reactor. Figure 1 shows a schematic diagram of the reactor.

Conversion of beef tallow was conducted by 25 g of beef tallow was put in the reactor and added catalyst MgONPs with the catalyst to feed weight ratio 2% and 4% compared with MgO commercial with the catalyst to feed weight ratio 4%, then heated from room temperature to 300 °C for 60 min. The formed gases flow out from the reactor through a cooled condenser. Figure 2 shows the experimental procedure conversion of beef Tallow to biofuel. Liquid products are analyzed using gas chromatography-mass spectrometry (GCMS, Perkin Elmer Clarus 600). Identified the compounds in liquid products using the NIST data library. The relative amount of each chemical compound in the liquid products was determined according to the percentage peak area (individual peak area/total peak area)

(Fan et al., 2017; Luo et al., 2016; Na et al., 2010). The product yield was obtained from the weight of liquid and residues. The gaseous product was calculated from the different weights of feedstock (tallow) with liquid products and residue.

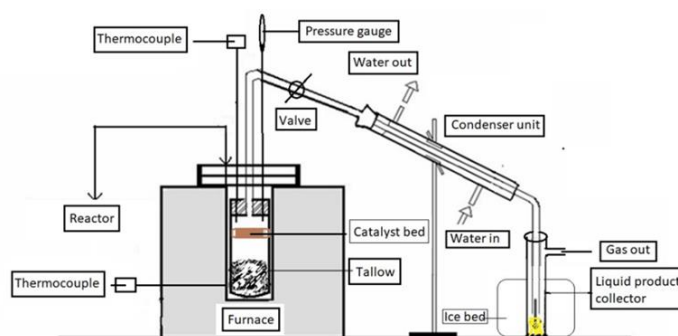


**Figure 1** The schematic diagram reactor system

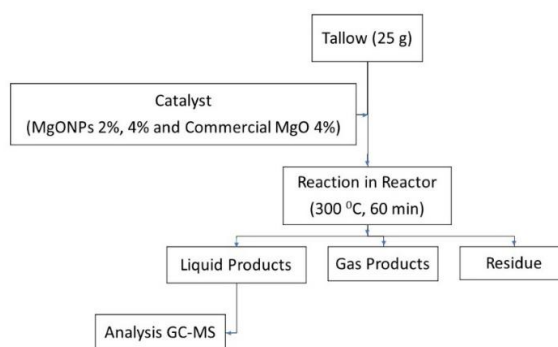


**Figure 2** Experimental procedure conversion of beef Tallow to biofuel

### 3. Results and Discussion

#### 3.1. Analysis of MgONPs Colloid using UV-Vis Spectrophotometer

The UV-Vis absorption spectrum of the synthesized MgONPs colloid at 60, 120, 180, and 240 min can be seen in Figure 3. UV-Vis spectrum analysis can confirm the MgONPs formation. Colloidal MgONPs have specific absorption peaks at wavelengths of 260–280 nm (Moorthy et al., 2015). UV-Vis spectrophotometer Observations were performed when mixing the  $\text{Mg}(\text{NO}_3)_2$  precursor with ZOE. The results showed that the longer reaction time shows the absorbance value in  $\lambda_{\text{max}} = 279$  nm increased due to the MgONPs formation. According to Moorthy et al. (2015), the 260 – 280 nm range is a UV-Vis absorption peak specific to MgONPs. This study obtained specific peaks at  $\lambda_{\text{max}} = 279$  nm, which can be proposed as a specific peak formation of MgONPs.

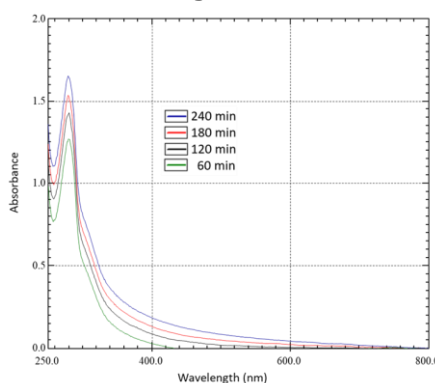


**Figure 3** The UV-Vis absorption spectra of MgONPs colloid at various reaction times

### 3.2. MgONPs Characterization

Characterization using UV-Vis DRS is done to find an optical band gap energy value of MgONPs. According to Badar et al. (2012), the bandgap energy value of MgONPs is 5.0 – 6.2 eV, and for MgO bulk, around 7.8 eV. This study showed the MgONPs bandgap energy of 6.0 eV, and the result is still in the range of the MgONPs bandgap.

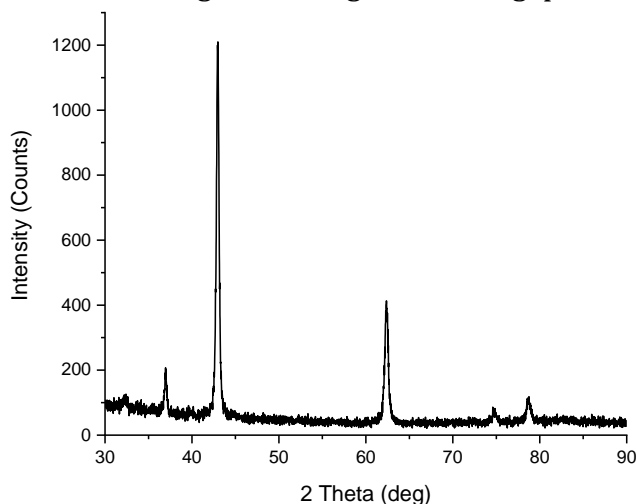


**Figure 4** XRD pattern of MgONPS

Analysis using XRD was conducted to confirm the crystal structure of the synthesized MgONPs, as shown in Figure 4. The diffraction spectrum reflects the crystallinity of MgONPs. The top three peaks ( $2\theta$ ) of MgONPs were at 36.92; 42.90; and 62.29 and can be indexed with the MgO periclase structure (JCPDS Card No: 78-0430). No peak characteristics of MgOH,  $Mg(NO_3)_2$ , and others were detected in the spectrum, indicating the precursor had been converted entirely to MgO. The crystallite size of the MgONPs was determined based on the Scherrer equation is about 27.1 nm. Particle size measurement was done using PSA by dispersing of MgONPs in the water showing the dominant particle size distribution of 79.25 nm, as seen in Figure 5.

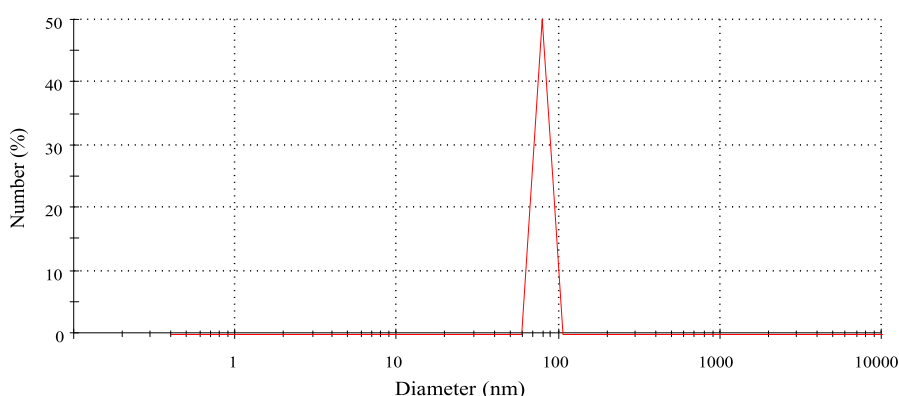


**Figure 5** Particle size distribution of MgONPs using PSA

MgONPs characterization using TEM can be seen in Figure 6, showing the hexagonal shape. MgONPs characterization is further confirmed using SEM to show the morphology, as seen in Figure 7. The determining elements composition by EDX shows the MgO composition is 45.96 % Mg and 54.04% O, equivalent to a ratio of 1:1 according to the MgO molecule. Surface area analysis was done using Branauer-Emmet-Teller (BET) methods and desorption using Barrett, Joyner, and Halenda (BJH). This method shows the pore radius and the pore size of the adsorption-desorption isotherm. Based on BET analysis of the

synthesized MgONPs, the BET Surface area of 12.84 m<sup>2</sup>/g and average pore size of 12.76 nm were obtained. According to Oh et al. (2011), the calcination of MgO at a higher temperature decreased the surface area because of sintering. The BET surface areas of MgO with calcination at 400°C, 600°C, and 800°C were 41.1 m<sup>2</sup>/g, 32.1 m<sup>2</sup>/g, and 8.1 m<sup>2</sup>/g (Oh et al., 2011). These results are not much different from this study.

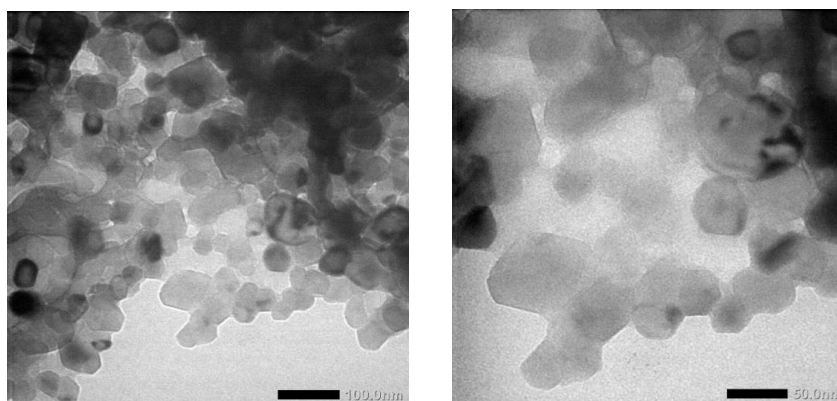


**Figure 6** TEM images of MgONPs

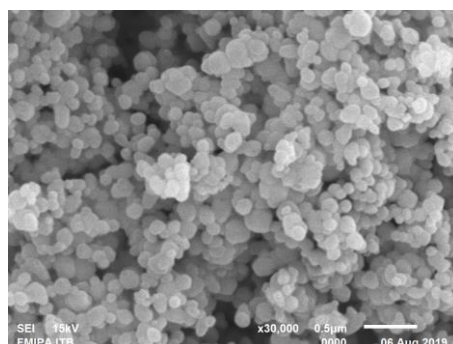


**Figure 7** SEM image at 30.000 magnification

### 3.3. The Conversion of Beef Tallow to Biofuel using MgONPs Catalyst

The main content of beef tallow are octadecanoic acid, 11-octadecenoic acid, and hexadecanoic acid (Riyadhi et al., 2020). The activity test of MgONPs catalyst on the conversion reaction of beef tallow resulted in the gases, liquid fractions, and black paste residue (Figure 8). Liquid products produced from the catalytic process are bright yellow and do not freeze at 0°C. The number of gases produced from beef tallow conversion using MgONPs catalyst (4%) is more than using commercial MgO catalyst (4%) (Figure 8).

Figure 9 shows the analysis of the liquid products using GC-MS. The results are grouped into three fractions, namely gasoline (C<sub>5</sub>-C<sub>11</sub>), kerosene (C<sub>12</sub>-C<sub>15</sub>), and diesel (C<sub>16</sub>-C<sub>26</sub>) (Demirbas, 2015). The compositions of liquid products depend on the percent of MgONPs catalysts. The more catalysts are used, the more gasoline and kerosene products, while the diesel product decreases. The amount of gasoline and kerosene products of liquid fraction resulting from the conversion of beef tallow using MgONPs (4%) is more than using commercial MgO (4%), contrary for the diesel product (Figure 9).

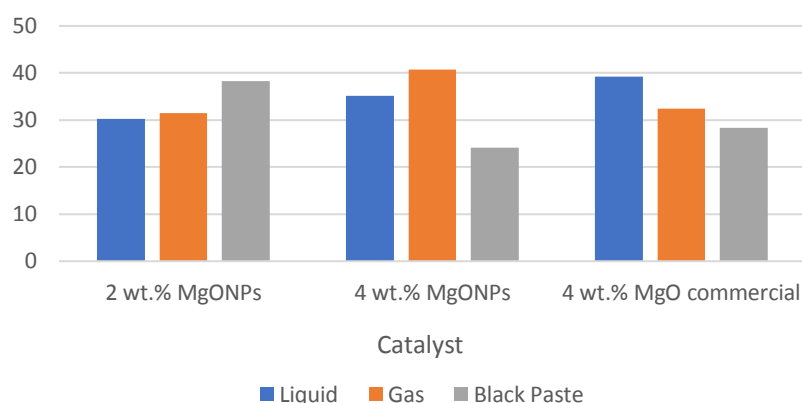


**Figure 8** Products distribution of beef tallow conversion using MgONPs and commercial MgO catalysts

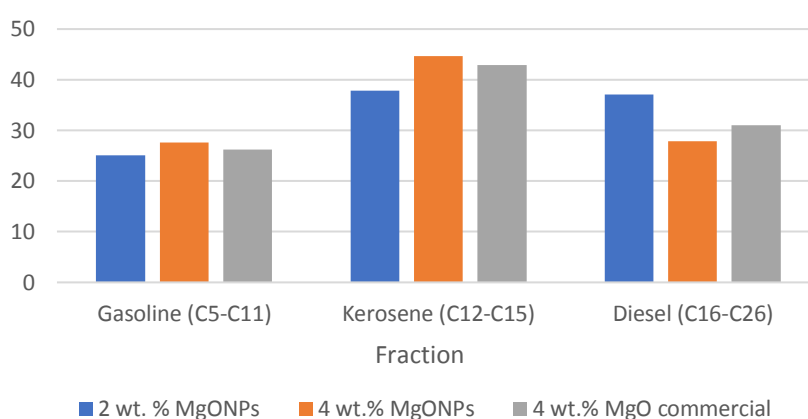


**Figure 9** Products composition based on petroleum range of liquid fraction

The cases are due to the cracking process so MgONPs catalyst role is better than commercial MgO. Catalytic cracking causes large molecules to conversion to smaller molecules resulting in more gases and liquid fractions. MgONPs catalyst can accelerate catalytic activity due to small particle size and high surface area. When the particle size decreases, the surface area increases, and thus the activity increases (Gajengi et al., 2017). The more catalysts are used, the more catalytic cracking reactions occur. Besides the reaction of catalytic cracking also occurred the decarboxylation of beef tallow, and no found carboxylic acid group compounds of fatty acids were using 4 % of MgONPs catalysts. The reaction using 2 % of MgONPs catalysts still found the carboxylic acid group compounds of 0.87% (Figure 10). The deoxygenation of fatty acids can occur through the mechanisms of decarbonylation or decarboxylation using catalysts (Dawes et al., 2015; Dragu et al., 2015; Wu et al., 2016).

Figure 10 shows the organic compounds of the liquids fraction. The dominant liquid products using 2% MgONPs catalyst are alkanes (56.73%), ketones (13.03%), cyclic compounds (11.34%), and alkenes (10.10%), while the dominant products using 4% MgONPs are alkanes (62.85%), cyclic compounds (18.77%), ketones (7.98%) and alkenes (5.54%) due to the catalytic deoxygenation from the ketones, ethers, esters, aldehydes, and carboxylic acids and also the catalytic cracking from the alkenes.

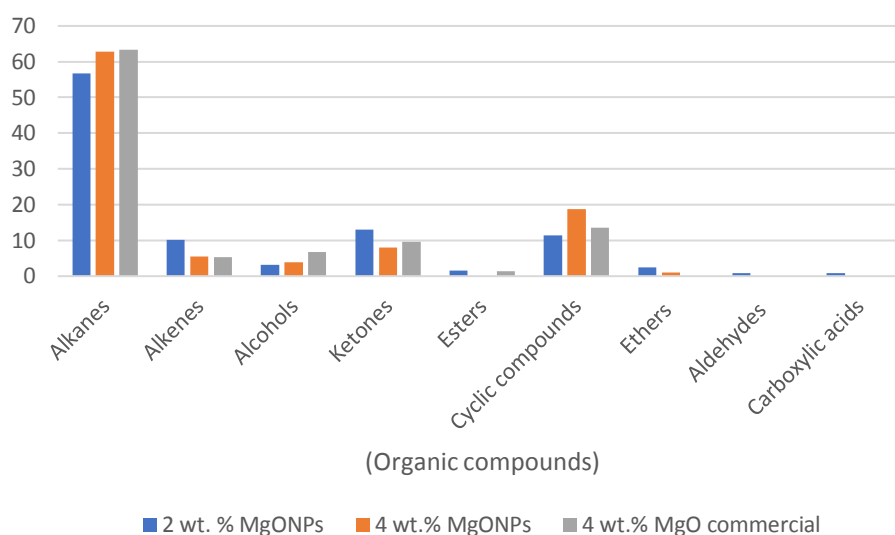


**Figure 10** The organic compounds composed of the liquid fraction

**Table 1** GC/MS percentage peak areas of major liquid products

Formula	Compound	Percentage peak area (%) (catalysts)*		
		2 wt.% MgONPs	4 wt.% MgONPs	4 wt.% MgO commercial
C <sub>15</sub> H <sub>32</sub>	Pentadecane	10.42	11.02	10.71
C <sub>17</sub> H <sub>36</sub>	Heptadecane	10.07	9.88	9.31
C <sub>13</sub> H <sub>28</sub>	Tridecane	5.78	6.62	6.49
C <sub>14</sub> H <sub>30</sub>	Tetradecane	5.01	6.00	6.07
C <sub>12</sub> H <sub>26</sub>	Dodecane	4.24	5.05	5.21
C <sub>16</sub> H <sub>34</sub>	Hexadecane	4.26	4.89	4.92
C <sub>11</sub> H <sub>24</sub>	Undecane	3.65	4.29	4.41
C <sub>8</sub> H <sub>18</sub>	Octane	4.15	3.94	4.14
C <sub>17</sub> H <sub>34</sub> O	2-Heptadecanone	3.00	3.73	3.95
C <sub>9</sub> H <sub>20</sub>	Nonane	3.31	3.42	3.54
C <sub>10</sub> H <sub>22</sub>	Decane	2.87	3.29	3.35

\*Percentage peak area = individual peak area/total peak area

The main content of beef tallow are hexadecanoic acid and octadecanoic acid (Riyadhi et al., 2020) and the major products of beef tallow conversion are pentadecanes and heptadecane (Table 1) indicates that decarboxylation reaction occurs from the hexadecanoic acid and octadecanoic acid (Figure 11). According to Perera et al. (2015), the reaction between MgO and carboxyl group (–COOH) in fatty acid begins with physisorption by van der Waals force on the surface then while continuing to perform the chemisorption which involves a chemical reaction between the surface MgO and carboxyl group (–COOH). Chemisorption of carboxyl groups on the MgO surface causes decarboxylation (Perera et al., 2015).

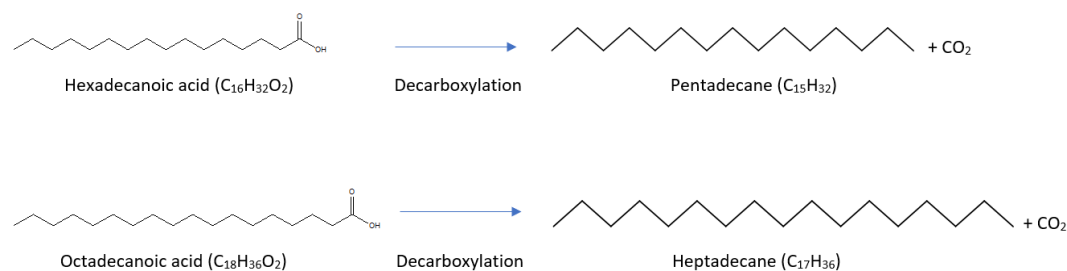


**Figure 11** Decarboxylation reaction of hexadecanoic acid and octadecanoic acid

Proposed all reactions for conversion of beef tallow to bio-oil are decarboxylation, cracking decarbonylation, aromatization, and isomerization (Maher et al., 2008; Santillan-Jimenez & Crocker, 2012).

#### 4. Conclusions

MgONPs have been successfully synthesized using the green synthesis method from magnesium nitrate precursor and white ginger extract as the weak base source and capping agents. The results of MgONPs characterization show the hexagonal shape and the nano size of 79.25 nm. MgONPs catalytic activity of the beef tallow conversion at low temperatures (300°C) for 60 min showed that a higher catalyst resulted in higher gasses, gasoline, and kerosene products, contrary to diesel products. The liquid fractions consist of gasoline, kerosene, and diesel products. The amount of gasoline, kerosene, and cyclic compounds of liquid fraction resulting from beef tallow conversion using MgONPs catalyst is more than the commercial MgO catalyst. MgONPs catalyst encourages more cracking process than commercial MgO. Higher MgONPs catalysts ratio also indicated higher alkanes and cyclic compound products due to the catalytic deoxygenation and cracking process. The primary compounds of the liquid product are pentadecane and Heptadecane, which indicates that decarboxylation reaction occurs from hexadecanoic acid and octadecanoic acid. Tallow and vegetable oils have similar fatty acid content, so catalyst MgONPs can also convert vegetable oils to biofuel.

#### Acknowledgements

The Indonesia Endowment Fund for Education funded this research, Ministry of Finance, Republik Indonesia (LPDP Kementerian Keuangan RI) for the Scholarships and Research Grants (No. S-168/LPDP.3/2017).

#### References

- Abdallah, Y., Ogunyemi, S.O., Abdelazez, A., Zhang, M., Hong, X., Ibrahim, E., Hossain, A., Fouad, H., Li, B., Chen, J., 2019. The Green Synthesis of MgO Nano-Flowers Using *Rosmarinus officinalis* L. (Rosemary) and the Antibacterial Activities against *Xanthomonas oryzae* pv. *oryzae*. *BioMed Research International*, Volume 2019, pp. 1–8
- Badar, Nurhanna, Chayed, N.F., Rusdi, R., Kamarudin, N., Kamarulzaman, N., 2012. Band Gap Energies of Magnesium Oxide Nanomaterials Synthesized by the Sol-Gel Method. *Advanced Materials Research*, Volume 545, pp. 157–160
- Dawes, G.J.S., Scott, E.L., Le Nôtre, J., Sanders, J.P.M., Bitter, J.H., 2015. Deoxygenation of Biobased Molecules by Decarboxylation and Decarbonylation - A Review on The Role of Heterogeneous, Homogeneous and Bio-Catalysis. *Green Chemistry*, Volume 17(6), pp. 3231–3250

- Demirbas, A. 2015. Recovery of Gasoline and Diesel Range Hydrocarbons from Waste Vegetable Oils. *Petroleum Science and Technology*, Volume 33(19), pp. 1703–1711.
- Dickerson, T., & Soria, J., 2013. Catalytic Fast Pyrolysis: A review. *Energies*, Volume 6(1), pp. 514–538
- Diez, V.K., Apesteeguía, C.R., Di Cosimo, J.I., 2000. Acid-Base Properties and Active Site Requirements for Elimination Reactions on Alkali-Promoted MgO Catalysts. *Catalysis Today*, Volume 63(1), pp. 53–62
- Dragu, A., Kinayyigit, S., García-Suárez, E.J., Florea, M., Stepan, E., Velea, S., Tanase, L., Collière, V., Philippot, K., Granger, P., Parvulescu, V.I., 2015. Deoxygenation of Oleic Acid: Influence of The Synthesis Route of Pd/Mesoporous Carbon Nanocatalysts onto Their Activity and Selectivity. *Applied Catalysis A: General*, Volume 504, pp. 81–91
- Fan, L., Chen, P., Zhang, Y., Liu, S., Liu, Y., Wang, Y., Dai, L., Ruan, R., 2017. Fast Microwave-Assisted Catalytic Co-Pyrolysis of Lignin and Low-Density Polyethylene with HZSM-5 and MgO for Improved Bio-Oil Yield and Quality. *Bioresource Technology*, Volume 225, pp. 199–205
- Gajengi, A.L., Sasaki, T., Bhanage, B.M., 2017. Mechanistic Aspects of Formation of MgO Nanoparticles under Microwave Irradiation and its Catalytic Application. *Advanced Powder Technology*, Volume 28(4), pp. 1185–1192
- Gasnov, A.G., Azizov, A.G., Aliyeva, S.T., Gasanova, G.D., Guseynov, N.S., Khalilova, S.R., Ayyubov, I.G., 2013. Application of Magnesium and Titanium Oxides as Catalysts in Reaction Decarboxylation of Acids. *Processes of petrochemistry and oil-refining*. Volume 14(55), pp. 169–174
- Judith Vijaya, Jayaprakash, N., Kombaiah, K., Kaviyarasu, K., Kennedy, L.J., Ramalingam, R.J., Lohedan, H.A. Al, Mohammed, M.A.V., Maaza, M., 2017. Bioreduction Potentials of Dried Root of Zingiber officinale for A Simple Green Synthesis of Silver Nanoparticles: Antibacterial Studies. *Journal of Photochemistry and Photobiology B: Biology*, Volume 177, pp. 62–68
- Khromova, S.A., Smirnov, A.A., Selishcheva, S.A., Kukushkin, R.G., Dundich, V.O., Trusov, L.I., Yakovlev, V.A., 2013. Magnesium-Containing Catalysts for The Decarboxylation of Bio-Oil. *Catalysis in industry*, Volume 5(3), pp. 260–268
- Leong, S.K., Lam, S.S., Ani, F.N., Ng, J.H., Chong, C.T., 2016. Production of Pyrolyzed Oil from Crude Glycerol using A Microwave Heating Technique. *International Journal of Technology*, Volume 7(2), pp. 323–331
- Luo, Y., Guda, V.K., Hassan, E.B., Steele, P.H., Mitchell, B., Yu, F., 2016. Hydrodeoxygenation of Oxidized Distilled Bio-Oil for The Production of Gasoline Fuel Type. *Energy Conversion and Management*, Volume 112, pp. 319–327
- Maher, K.D., Kirkwood, K.M., Gray, M.R., Bressler, D.C., 2008. Pyrolytic Decarboxylation and Cracking of Stearic Acid. *Industrial and Engineering Chemistry Research*, Volume 47(15), pp. 5328–5336
- Moorthy, S.K., Ashok, C.H., Rao, K.V., Viswanathan, C., 2015. Synthesis and Characterization of MgO Nanoparticles by Neem Leaves Through Green Method. *Materials Today: Proceedings*, Volume 2(9), pp. 4360–4368
- Muharam, Y., Soedarsono, J.A., 2020. Hydrodeoxygenation of Vegetable Oil in a Trickle Bed Reactor for Renewable Diesel Production. *International Journal of Technology*, Volume 11(7), pp. 1292–1299
- Na, J.G., Yi, B.E., Kim, J.N., Yi, K.B., Park, S.Y., Park, J.H., Kim, J.N., Ko, C.H., 2010. Hydrocarbon Production from Decarboxylation of Fatty Acid without Hydrogen. *Catalysis Today*, Volume 156(1–2), pp. 44–48

- Nasikin, M., Susanto, B.H., Hirsaman, M.A., Wijanarko, A., 2009. Biogasoline from Palm Oil by Simultaneous Cracking and Hydrogenation Reaction over Nimo / zeolite Catalyst. *World Applied Sciences Journal*, Volume 5, pp. 74–79
- Natewong, P., Murakami, Y., Tani, H., Asami, K., Natewonga, P., Murakamib, Y., Tanic, H., Asami, K., 2016. Effect of Support Material on MgO-Based Catalyst for Production of New Hydrocarbon Bio-Diesel. *American Scientific Research Journal for Engineering, Technology, and Sciences (ASRJETS)*, Volume 22(1), pp. 153–165
- Noruzi, M., 2015. Biosynthesis of Gold Nanoparticles using Plant Extracts. *Bioprocess and Biosystems Engineering*, Volume 38(1), pp 1–14
- Oh, H.-Y., Park, J.-H., Rhee, Y.-W., Kim, J.-N., 2011. Decarboxylation of Naphthenic Acid using Alkaline Earth Metal Oxide. *Journal of Industrial and Engineering Chemistry*, Volume 17, pp. 788–793
- Perera, D.C., Hewage, J.W., de Silva, N., 2015. Theoretical Study of Catalytic Decomposition of Acetic Acid on MgO Nanosurface. *Computational and Theoretical Chemistry*, Volume 1064, pp. 1–6
- Pugazhendhi, A., Prabhu, R., Muruganatham, K., Shanmuganathan, R., Natarajan, S., 2019. Anticancer, Antimicrobial and Photocatalytic Activities of Green Synthesized Magnesium Oxide Nanoparticles (MgONPs) using Aqueous Extract of Sargassum wightii. *Journal of Photochemistry and Photobiology B: Biology*, Volume 190, pp. 86–97
- Raaof, A., Al-naqqash, Z.A., Jawad, A.M., Muhsan, S.M., 2013. Evaluation of The Activity of Crude Alkaloids Extracts of Zingiber officinale Roscoe., Thymus vulgaris L. and Acacia arabica L. as coagulant agent in lab mice. *Biomedicine and Biotechnology*, Volume 1(2), pp. 11–16
- Riaz, H., Begum, A., Raza, S.A., Khan, Z. M.-U.-D., Yousaf, H., Tariq, A., 2015. Antimicrobial Property and Phytochemical Study of Ginger Found in Local Area of Punjab, Pakistan. *International Current Pharmaceutical Journal*, Volume 4(7), pp. 405–409
- Riyadhi, A., Yulizar, Y., Susanto, B.H., 2020. Catalytic Conversion of Beef Tallow with MgO derived from MgCO<sub>3</sub> for Biofuels Production. *IOP Conference Series: Materials Science and Engineering*
- Roh, H.-S., Eum, I.-H., Jeong, D.-W., Yi, B.E., Na, J.-G., 2011. The Effect of Calcination Temperature on The Performance of Ni/MgO–Al<sub>2</sub>O<sub>3</sub> Catalysts for Decarboxylation of Oleic Acid. *Catalysis Today*, Volume 164(1), pp. 457–460
- Santillan-Jimenez, E., Crocker, M., 2012. Catalytic Deoxygenation of Fatty Acids and Their Derivatives to Hydrocarbon Fuels via Decarboxylation/Decarbonylation. *Journal of Chemical Technology and Biotechnology*, Volume 87(8), pp. 1041–1050
- Sekoai, P.T., Naphtaly, C., Ouma, M., Petrus, S., Modisha, P., Engelbrecht, N., Bessarabov, D. G., Ghimire, A., 2019. *Application of nanoparticles in biofuels: An overview*. Volume 237, pp. 380–397
- Suresh, J., Pradheesh, G., Alexramani, V., Sundrarajan, M., Ig, S., 2018. Green Synthesis and Characterization of Hexagonal Shaped MgO Nanoparticles using Insulin Plant (Costus pictus D. Don) Leave Extract and its Antimicrobial as well as Anticancer Activity. *Advanced Powder Technology*, Volume 29(7), pp. 1685–1694
- Surya, R.M., Yulizar, Y., Cahyana, A.H., Apriandanu, D.O.B., 2021. One-pot Cajanus cajan (L.) Millsp. Leaf Extract-mediated Preparation of MgFe<sub>2</sub>O<sub>4</sub> Nanoparticles: Optical, Structural, Morphological And Particle Size Analyses. *Solid State Communications*, Volume 326, pp. 114170
- Susanto, B.H., Prakasa, M.B., Nasikin, M., Sukirno., 2016. Synthesis of Renewable Diesel from Palm Oil and Jatropha Curcas Oil Through Hydrodeoxygenation Using NiMo/ZAL. *International Journal of Technology*, Volume 7(8), pp. 1404–1411

- Velmurugan, P., Anbalagan, K., Manosathyadevan, M., Lee, K.-J., Cho, M., Lee, S.-M., Park, J.-H., Oh, S.-G., Bang, K.-S., Oh, B.-T., 2014. Green Synthesis of Silver and Gold Nanoparticles using Zingiber Officinale Root Extract and Antibacterial Activity of Silver Nanoparticles Against Food Pathogens. *Bioprocess Biosyst Eng*, Volume 37(10), pp. 1935–1943
- Vergheese, M., Vishal, S.K., 2018. *Green synthesis of Magnesium Oxide nanoparticles using Trigonella foenum-graecum leaf extract and its antibacterial activity*. Volume 7(3), pp. 1193–1200
- Wu, J., Shi, J., Fu, J., Leidl, J.A., Hou, Z., Lu, X., 2016. Catalytic Decarboxylation of Fatty Acids to Aviation Fuels over Nickel Supported on Activated Carbon. *Nature Publishing Group*, Volume 6, pp. 27820
- Yang, N., Li, F., Jian, T., Liu, C., Sun, H., Wang, L., Xu, H., 2017. Biogenic Synthesis of Silver Nanoparticles using Ginger (Zingiber Officinale) Extract and Their Antibacterial Properties Against Aquatic Pathogens. *Acta Oceanologica Sinica*, Volume 36(12), pp. 95–100
- Yulizar, Y., Bakri, R., Oky, D., Apriandanu, B., Hidayat, T., 2018. Nano-Structures & Nano-Objects ZnO / CuO Nanocomposite Prepared in One-Pot Green Synthesis using Seed Bark Extract of Theobroma cacao. *Nano-Structures & Nano-Objects*, Volume 16, pp. 300–305
- Zhang, A., Ma, Q., Wang, K., Liu, X., Shuler, P., Tang, Y., 2006. Naphthenic Acid Removal from Crude Oil Through Catalytic Decarboxylation on Magnesium Oxide. *Applied Catalysis*, Volume 303, pp. 103–109